

Clinical confocal microlaparoscope for real-time *in vivo* optical biopsies

Anthony A. Tanbakuchi

University of Arizona
Department of Radiology
Radiology Research Laboratories
1609 North Warren Avenue
Tucson, Arizona 85724
and
University of Arizona
College of Optical Sciences
1630 East University Boulevard
Tucson, Arizona 85724

Andrew R. Rouse

University of Arizona
Department of Radiology
Radiology Research Laboratories
1609 North Warren Avenue
Tucson, Arizona 85724

Joshua A. Udovich

University of Arizona
Department of Radiology
Radiology Research Laboratories
1609 North Warren Avenue
Tucson, Arizona 85724
and
University of Arizona
College of Optical Sciences
1630 East University Boulevard
Tucson, Arizona 85724

Kenneth D. Hatch

University of Arizona
Arizona Health Sciences Center
Department of Obstetrics and Gynecology
P.O. Box 245078
Tucson, Arizona 85724

Arthur F. Gmitro

University of Arizona
Department of Radiology
Radiology Research Laboratories
1609 North Warren Avenue
Tucson, Arizona 85724
and
University of Arizona
College of Optical Sciences
1630 East University Boulevard
Tucson, Arizona 85724
E-mail: gmitro@radiology.arizona.edu

1 Introduction

This paper describes the first clinical confocal microlaparoscope system. We describe the instrument and how it evolved during clinical testing. We present both *in vivo* and *ex vivo* results showing that the device has the ability to

Abstract. Successful treatment of cancer is highly dependent on the stage at which it is diagnosed. Early diagnosis, when the disease is still localized at its origin, results in very high cure rates—even for cancers that typically have poor prognosis. Biopsies are often used for diagnosis of disease. However, because biopsies are destructive, only a limited number can be taken. This leads to reduced sensitivity for detection due to sampling error. A real-time fluorescence confocal microlaparoscope has been developed that provides instant *in vivo* cellular images, comparable to those provided by histology, through a nondestructive procedure. The device includes an integrated contrast agent delivery mechanism and a computerized depth scan system. The instrument uses a fiber bundle to relay the image plane of a slit-scan confocal microlaparoscope into tissue. It has a 3- μm lateral resolution and a 25- μm axial resolution. Initial *in vivo* clinical testing using the device to image human ovaries has been done in 21 patients. Results indicate that the device can successfully image organs *in vivo* without complications. Results with excised tissue demonstrate that the instrument can resolve sufficient cellular detail to visualize the cellular changes associated with the onset of cancer. © 2009 Society of Photo-Optical Instrumentation Engineers. [DOI: 10.1117/1.3207139]

Keywords: endoscopy; confocal optics; fluorescence; medical imaging; microscopy; real-time imaging.

Paper 09055PR received Feb. 17, 2009; revised manuscript received Jun. 19, 2009; accepted for publication Jun. 22, 2009; published online Aug. 25, 2009. This paper is a revision of a paper presented at the SPIE conference Endoscopic Microscopy IV, January 2009, San Jose, California. The paper presented there appears (unrefereed) in SPIE Proceedings Vol. 7172.

nondestructively resolve cellular detail and has the potential to diagnose cancer *in situ*.

Cancer frequently goes undetected until it reaches a late, difficult-to-treat, stage. Cancers that develop in epithelial cells (carcinomas) are the most common type of malignancy, and they account for 90% of all human cancers.¹ Development of imaging devices that can more thoroughly interrogate epithelial surfaces for abnormalities will enable earlier detection of

Address all correspondence to: Arthur F. Gmitro, Department of Radiology, and College of Optical Sciences, University of Arizona, Tucson, AZ 85724. Tel. 520-626-4720; Fax: 520-626-3893; E-mail: gmitro@radiology.arizona.edu



Fig. 1 The microlaparoscope system imaging the epithelial surface of an ovary during surgery. In this image, the surgeon has located the left ovary using a wide-field laparoscope (for left display) and is inspecting the epithelial cells using the microlaparoscope via the second display from the left. The mobile cart is on the far right.

cancer, resulting in significant improvement in patient survival.

The most effective treatments in terms of patient outcomes, quality of life, and cost are those that target cancer during its early development, before it has metastasized. Early diagnosis, when the disease is still localized at its origin, results in very high cure rates—even for cancers that typically have poor prognosis. Early detection provides the physician with more treatment options and the ability to use less invasive methods. Unfortunately, many cancers are not found until later stages due to inadequate detection methods or low-sensitivity diagnostic techniques.

Initial detection and diagnosis of cancer is frequently based on biopsies. Small samples of tissue are removed, and a pathologist makes a diagnosis using thin sections of stained and processed tissue. Since biopsies require removal of the tissue, only a limited number can be taken. Sampling error plays a significant role in achieving accurate early detection of cancer. Development of devices that can nondestructively interrogate epithelial surfaces for abnormalities would reduce sampling error.

Many groups are investigating new technologies to nondestructively image tissue at high resolution for the early diagnosis of cancer. Some of the promising methods are confocal microscopy,^{2–10} two-photon microscopy,^{11,12} spectroscopy,^{13–18} and optical coherence tomography (OCT).^{19–25}

Conventional bright-field microscopy plays a central role in the diagnosis of disease from carefully prepared biopsy slides. Bright-field images of bulk tissue appear blurry due to simultaneous collection of out-of-focus planes. Improved imaging of thick samples can be achieved with confocal microscopy. Confocal images of bulk tissue are sharp because light from out-of-focus planes is rejected via a confocal aperture.

Since the confocal microscope alleviates the need for cutting tissue into thin sections, it has significant potential for imaging of tissue *in situ*. However, a standard confocal microscope is a large device that is not well suited for *in vivo*

assessment of epithelial surfaces inside the human body. We have previously reported on technology developed to enable *in vivo* confocal imaging using a coherent fiber optic bundle.^{26–30} In this paper, we describe development of a confocal microlaparoscope.

A confocal microlaparoscope offers the potential for cellular imaging of a wide range of laparoscopically accessible organs. Almost every organ in the human body can be accessed using a laparoscope via a small incision.³¹ Organs that can be accessed in this manner include the stomach, intestines, pancreas, liver, esophagus, spleen, kidneys, peritoneal wall, bladder, gall bladder, lymph nodes, reproductive organs in females, and prostate in men. Laparoscopic surgery has significant advantages over open surgery. It minimizes the overall trauma to the skin and muscles, patient recovery time is shorter, and the infection rate is significantly reduced.

In the following sections, we discuss the four-year development of a mobile confocal microlaparoscope imaging system. To demonstrate the device's potential, we present *in vivo* and *ex vivo* human imaging results.

2 Clinical Confocal Microlaparoscope System

We have developed a complete clinical confocal microlaparoscope system that can be wheeled into an operating room and set up to image within a few minutes. The system consists of a confocal microlaparoscope (hereafter referred to as a microlaparoscope) connected to a mobile cart housing an optical scan unit (OSU) and control systems. Once the system is running, the surgeon can interrogate regions of interest with the microlaparoscope; view live cellular images on the screen; and selectively record videos, depth scans, multispectral images, and still frames. Figure 1 shows the instrument in use in the surgical suite. The mobile cart is on the right, and the surgeon using the microlaparoscope is in the middle looking toward the left, where the gross anatomy is visible on a standard wide-field laparoscope screen. Directly adjacent to this

Table 1 System specifications.

Lateral resolution	3 μm
Axial resolution	25 μm
Collection elements (pixels)	30,000
Frame rate	30 fps
Excitation wavelength	488 nm
Spectral collection (150 spectral images)	6 s
Average spectral resolution	6 nm
Spectral collection	500 to 750 nm
Port compatibility	5 mm trocar
Dye delivery precision	50 nL
Numerical aperture in tissue	0.46
Micro-objective magnification	1.5
Chromatic correction	488 to 660 nm
Maximum imaging depth	200 μm
Field of view	450 μm

screen is another display showing the live cellular images from the microlaparoscope system.

The microlaparoscope provides live images of excited fluorescence at 30 frames per second with an optical resolution of 3 μm laterally and 25 μm axially. The system frame rate is fundamentally limited by the acquisition rate of the CCD camera used for detection. Fluorescent contrast agents are delivered locally to the field of view using an integrated contrast agent delivery system. Using controls on the microlaparoscope, the surgeon can adjust focus from the nominal epithelial position down to an optical limit of 200 μm below the surface. Table 1 provides a detailed listing of the system's specifications.

The evolution from a laboratory system^{26,28–30} to a successful surgical system entailed significant translational research over a four-year period.^{32–35} The work can be broken into two major areas: (1) the development of a mobile cart with a miniaturized confocal scan assembly (the OSU) and surgical control system and (2) the development of the clinical microlaparoscope. Both areas presented major challenges. The mobile cart required a redesign of the OSU and a change of the laser excitation system from a water-cooled gas laser to a small air-cooled solid-state laser. Making the microlaparoscope easy to use entailed significant developments to tightly integrate the focus and dye delivery systems to ensure quick and reliable response. In addition, the device had to be sterilizable, fit inside standard surgical trocars, and be safe to use inside a patient.

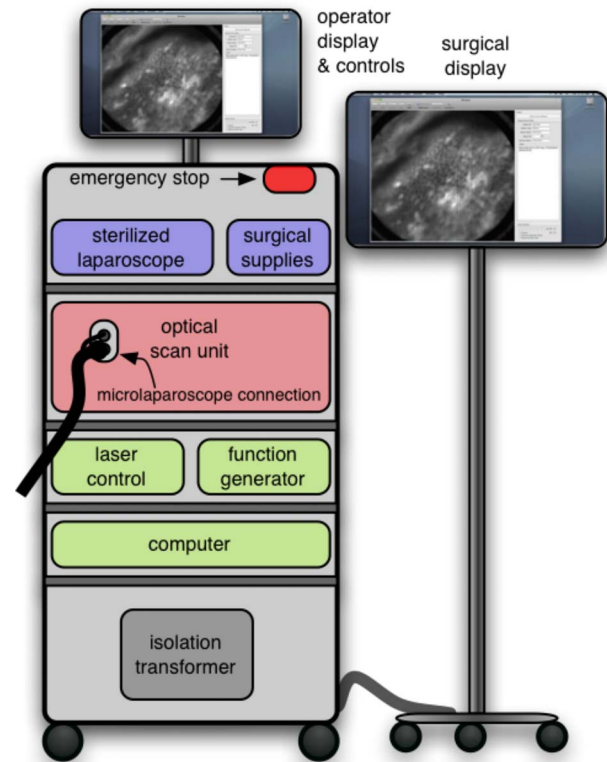


Fig. 2 Mobile microlaparoscope system. The mobile cart (left) houses the optical scan unit (OSU), surgical supplies, laser source, control systems, computer, and operator controls. The microlaparoscope cable connects to the OSU. The secondary display (right) is placed next to the operative field for live *in vivo* imaging.

In the following sections, we describe the mobile cart, the associated systems that it houses, and the functions that it provides. Then we will discuss the evolution of the microlaparoscope, beginning with the early prototypes and ending with the state-of-the-art instrumentation currently being used in human clinical trials. Details concerning the integrated in-handle axial focus and contrast agent delivery systems are also presented.

2.1 Mobile Cart

The mobile cart houses the OSU and the control systems. The instrumentation fits on a standard endoscopy cart that has a 61 cm by 41 cm footprint. Figure 2 depicts the components on the mobile cart. The top shelf houses the sterile microlaparoscope and the surgical supplies that are used during the imaging procedure. The microlaparoscope cable connects to the OSU located on the second shelf. The third and fourth shelves house the laser, function generator, and computer. The bottom shelf houses a medical-grade isolation transformer. The operator display and controls for collecting data during surgery are located on a platform at standing height. A second mobile display is placed next to the operative field for viewing nearby the surgeon.

The system has been designed to streamline all operations during surgery. Once the system is plugged in and the safety interlocks engaged, the system starts, and all hardware is initialized. Hardware initialization includes the solid-state laser,

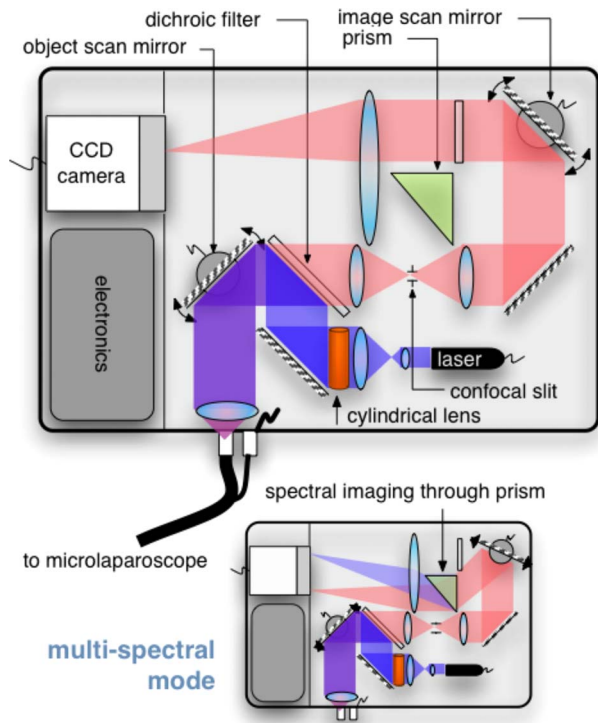


Fig. 3 Diagram of the OSU. The top portion illustrates the standard grayscale mode of operation. A 488-nm laser is anamorphically shaped into a line and scanned onto the coherent fiber bundle in the microlaparoscope. The excited signal re-enters the system, is descanned, and is filtered through a confocal slit. The light is rescanned onto a two-dimensional 2-D CCD camera. In the spectral imaging mode (bottom inset), the image scan mirror is turned to its extreme position, redirecting the light through a dispersing prism.

camera, dye delivery system, focus system, and function generator for scan mirror control. After the automatic initialization, the operator is presented with the software control interface for live imaging.

2.1.1 Optical scan unit

Miniaturization of the OSU required a redesign of the previous bench-top system. By simplifying the optical layout and integrating the multispectral imaging segment into a common collection path,³⁶ we were able to fit the whole scan system into a 50 cm by 30.5 cm housing. The housing also integrates the scan mirror power supply and control electronics, which were external in the previous system.

The components of the OSU are shown in Fig. 3. The top of the figure shows how the system operates in the standard grayscale imaging mode. In this mode, a 488-nm solid-state laser beam is expanded and anamorphically shaped into a line via a cylindrical lens. The laser light is then reflected into the image path by a dichroic filter, imaged to a line by a microscope objective, and scanned by the object scan mirror across the coherent fiber bundle face in the microlaparoscope's proximal connector.

Tissue fluorescence is collected back through the microlaparoscope and descanned by the object scan mirror. The dichroic filter passes the fluorescence signal, which is focused down onto a stationary confocal slit. The light exiting the slit

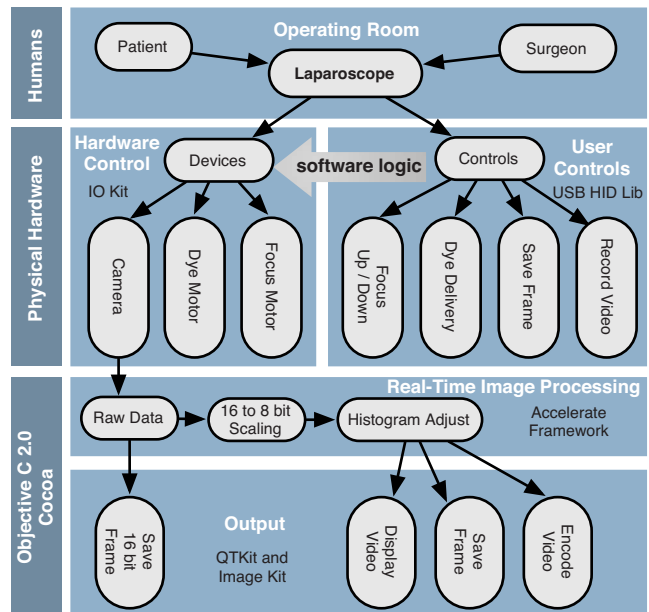


Fig. 4 Flow diagram illustrating how the software integrates the hardware, live output, and data acquisition components of the microlaparoscope system.

is recollimated and rescanned using the image scan mirror. An emission filter removes residual excitation light. The beam is refocused back into a line that sweeps across the camera to build up a two-dimensional (2-D) image every thirtieth of a second.

In addition to 2-D grayscale imaging, the system can also collect multispectral data.^{27,29,36} This multispectral mode is activated in a fraction of a second via a software actuation button that deflects the image scan mirror to its extreme position (shown in the bottom of Fig. 3). During spectral collection, the image scan mirror is held stationary. The light passes through a prism dispersing the signal across the CCD. The CCD camera records spectral information in the direction perpendicular to the slit and one dimension of spatial data in the dimension parallel to the slit. The second spatial dimension of the image is collected over time by recording multiple frames as the object scan mirror is slowly stepped. The complete spectral data collection procedure executes in a few seconds. Once spectral collection is complete, the system reverts back to real-time grayscale operating mode.

2.1.2 Software control system

A software package that interfaces with the data collection devices and the system controls was written using Objective C 2.0 and Cocoa with automatic garbage collection on Mac OS X. Figure 4 provides a general overview of the software and hardware interface. The software links the surgical controls on the microlaparoscope to the control systems that manage contrast agent delivery, focus, and data acquisition. Parallel processing allows the software to run smoothly while live images are acquired, processed, and encoded at 30 frames per second. A custom image processing memory pool class enables efficient resource management under automatic garbage collection.

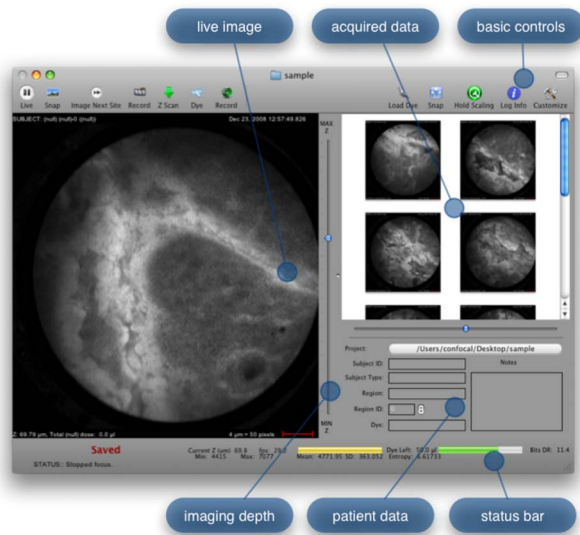


Fig. 5 Software control system interface. The main window provides the live view and basic controls to run the system. The right side contains previews of data acquired during the procedure along with patient data.

Figure 5 shows the software interface. It provides a simple interface for viewing and collecting live images during the surgical procedure. The software has controls to (1) start live acquisition, (2) save the current frame, (3) record video, (4) deliver dye, (5) load dye, and (6) adjust image display. In addition to the basic controls, the system also records procedure and patient information, which is archived with each image. System information, including image dynamic range and imaging depth, are also visible. During operation, the surgeon can easily see real-time imagery on the surgical display (shown in Fig. 1) along with the instrument’s current status. Contrast agent delivery, focus, and data acquisition can be initiated by the surgeon via integrated controls on the third-generation microlaparoscope handle, described in the next section.

2.2 Confocal Microlaparoscopes

Use of the surgical microlaparoscope entails placing the distal end in contact with the tissue, locally delivering fluorescent contrast agents to the field of view, adjusting focus, and collecting the resultant fluorescent confocal image.

To create the surgical microlaparoscope, we had to develop (1) a reliable focus mechanism, (2) a localized contrast agent delivery system, and (3) an ergonomic sterilizable housing with surgical controls compatible with a 5-mm-diam trocar instrument port. The development process encompassed three generations of instruments, with the final version meeting all of the requirements. Table 2 summarizes the key properties of the three designs.

In all three designs, the microlaparoscope contains a 30,000-element fiber bundle connected via a subminiature version A (SMA) connector to the OSU. The OSU generates a line of laser illumination that sweeps across the proximal face of the fiber. The fiber bundle spatially relays the illumination pattern to the distal end of the fiber bundle, where a miniature 0.46 NA objective lens³⁰ images the illumination line to the desired tissue depth. Image depth is controlled by adjusting the axial spacing between the fiber bundle and the miniature objective lens. Contrast agent is locally delivered to the tissue through the microlaparoscope. The excited fluorescent signal is collected by the miniature lens and relayed back through the fiber bundle into the OSU.

2.2.1 First-generation design

The first-generation design—depicted in Fig. 6—utilized a sterilizable semirigid 5-mm-diam by 500-mm-long dual-lumen polycarbonate sleeve through which a nonsterile imaging catheter was inserted.³⁰ This simple design allowed us to rapidly move to clinical testing by creating a sterile housing for our existing 3-mm flexible imaging catheter. The polycarbonate also integrated a small secondary lumen to deliver dye locally to the field of view. The front end of the polycarbonate sleeve was sealed with a 160- μm -thick glass window. A 500- μm -diam secondary lumen, used to deliver contrast

Table 2 Comparison of key properties for the three generations of microlaparoscopes.

	First Generation	Second Generation	Third Generation
OSU connection	fixed	SMA	SMA
Cable length	1.2 m	6 m	6 m
Focus type	motorized	manual	motorized
Focus control location	cart	handle	handle
Focus precision	20 μm	5 μm	0.5 μm
Dye control location	cart	handle	handle
Dye precision	3 μL	1 μL	50 nL
Axial position recording	no	no	yes
z-scan capability	yes	no	yes

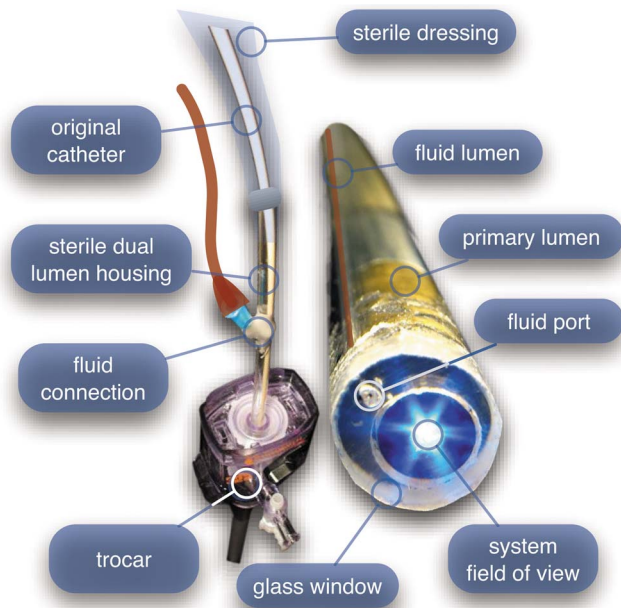


Fig. 6 First-generation microlaparoscope. The front end of the dual-lumen polycarbonate housing is shown on the right. The existing imaging catheter is inside the primary lumen, with the miniature objective flush against the glass window sealing the face. The secondary contrast agent fluid delivery lumen exits through a laser-drilled port in the glass face. The left side of the figure depicts the rear end of the polycarbonate housing passing into a 5-mm trocar port. The dye line and imaging catheter are connected to the rear end of the housing.

agent, ran parallel to the primary lumen. A 200- μm -diam hole in the window was placed over the secondary lumen, allowing contrast agent delivery to the tissue.

The rear end of the polycarbonate housing contained the couplings to mate the imaging catheter and the dye delivery line. In the operating room, the compression coupling of the sterilized polycarbonate housing was loosened, and the non-sterile imaging catheter was fed through the main 3.1-mm lumen until the miniature objective was in contact with the glass window. The fitting was tightened, and then a sterile plastic cover was slid back over the portion of the imaging catheter that was in the operative field. A Luer Lock fitting coupled the fluid lumen to a 0.58-mm medical-grade Teflon tubing that ran back to the mobile cart.

The 3-mm flexible catheter consisted of a miniature objective lens connected to durable polyetheretherketone (PEEK) tubing. The 30,000-element fiber optic bundle ran through the lumen of the PEEK tubing. Originally, focus was accomplished by a manual micrometer at the proximal end that moved the fiber bundle relative to the PEEK housing. However, focus control was unreliable due to an inexact fit of the fiber bundle inside the PEEK tubing. This resulted in hysteresis in the proximal movement of the fiber bundle relative to the fixed lens. Various methods were studied to improve the focus system.^{29,30,34} Ultimately, the manual focus micrometer was replaced by a computerized stepper motor. A hysteresis correction algorithm was developed to position the distal fiber face with an accuracy better than the system's axial resolution. Figure 7 illustrates the ability of the first-generation focus system to image the epithelial surface of tissue (mouse

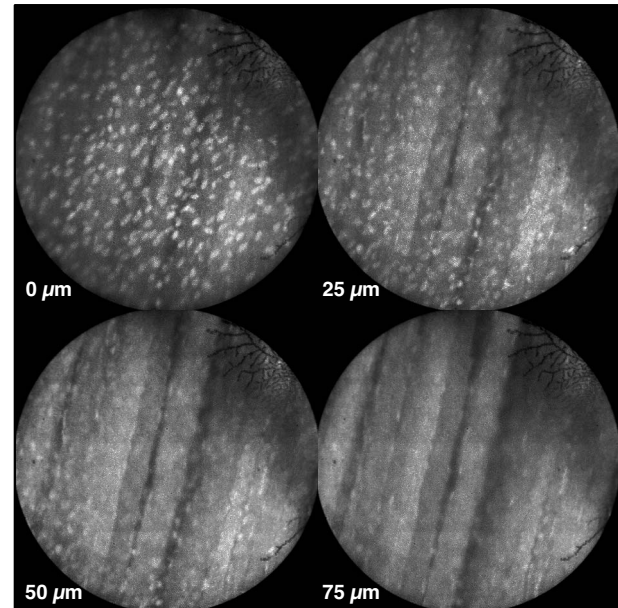


Fig. 7 Image sequence demonstrating first-generation focus control and the confocal properties of the OSU. Sequence shows the process of incrementally focusing from the epithelial layer (0 μm) down to the muscle layer of mouse peritoneal wall in 25- μm increments. (Circular field of view is 450 μm .)

peritoneal wall) and then to controllably focus the underlying tissue layers in 25- μm increments.

Dye delivery was accomplished by loading a syringe with fluorescent contrast agent. The syringe was then inserted into a syringe pump located on the mobile cart. The syringe was connected to the secondary lumen of the polycarbonate housing through 0.58-mm-diam medical-grade Teflon tubing. Software control of the syringe pump enabled delivery of 1- to 3- μL droplets of contrast agent onto the tissue surface near the field of view of the miniature objective. Figure 8 shows a photograph of the distal end of the microlaparoscope with a droplet of dye coming out through the hole in the glass window.

The device worked well using the 1.2-m-long imaging catheter. However, it was determined that a longer length imaging catheter was needed in the operating room. With the longer length catheter, the focus motor and the syringe pump were located far from the distal microlaparoscope tip, and

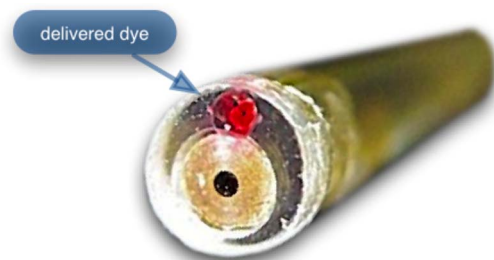


Fig. 8 Demonstration of contrast agent delivery in the first-generation system. Delivery time was approximately one second to deliver a 1- μL volume.

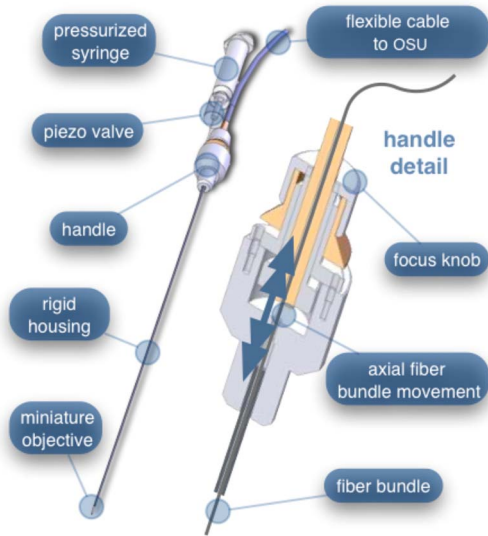


Fig. 9 The second-generation microlaparoscope. The overall device, shown on the left, incorporated a manual focus mechanism and an integrated dye delivery system that uses a piezo valve and a pressurized syringe. The right side shows a cross-section of the depth/focus knob built into the handle.

focus would drift during use. Delivery of small droplets of contrast agent was unreliable. The surgeon also noted that positioning the proximal tip accurately was difficult because the polycarbonate housing was not rigid enough.

2.2.2 Second-generation design

A second-generation device was developed to address the issues concerning device rigidity, focus drift, and reliability of contrast agent delivery across a 6-m-long connection between the microlaparoscope and the OSU. The second design abandoned the use of the existing flexible imaging catheter. To address the reliability issues of focus and dye delivery in a 6-m-long device, the controls for focus and dye delivery were located close to the distal tip. To address the rigidity issue, a rigid instrument was made using a stainless steel tube with an inner diameter matching the fiber bundle's outer diameter. Figure 9 shows a diagram of the second-generation microlaparoscope.

The miniature objective attached to the distal end of the 3-mm-diam rigid stainless steel tube. The fiber bundle ran through the 1 mm inside diameter of the rigid tube. To adjust focus, the fiber bundle moved axially relative to the fixed lens position. The tube and fiber bundle were held in place by a round handle containing a manual focus mechanism. Rotation of the handle knob resulted in precise movement of the proximal fiber face relative to the rigid tube. To deliver contrast agents, a 21-gauge hypodermic tube ran parallel to the 3-mm rigid tube. Both tubes were sealed inside medical-grade fluorinated ethylene-propylene (FEP) heat-shrink tubing, resulting in a final 5-mm outer diameter. At the distal tip, the hypodermic tube made a 90-deg bend, dispensing contrast agents at the edge of the imaging field. At the back end of the handle, the hypodermic tubing passed into a computer-controlled piezo valve immediately downstream from a pressurized syringe. A 6-m-long flexible cable ran from the handle to

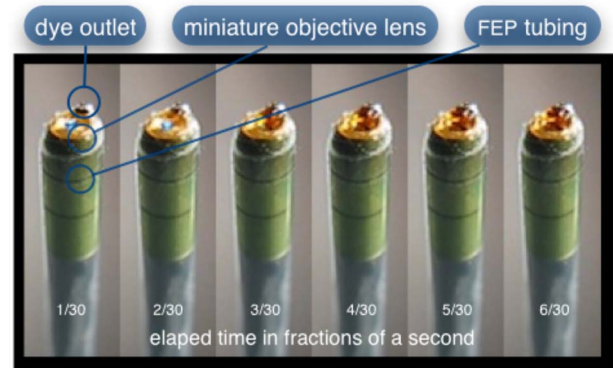


Fig. 10 Demonstration of the ability of the second-generation microlaparoscope to deliver small volumes of contrast agent to the field of view. In this sequence of images, the operator presses the dye delivery button and the dye is delivered to the distal tip via actuation of the piezo valve. The delivered volume in this example is approximately $1 \mu\text{L}$.

the OSU. The cable contained the fiber bundle and piezo valve electrical wires. The proximal end of the protective housing broke out into optical and electrical connectors. A standard SMA connector coupled the fiber bundle to the OSU.

Compared to the first-generation system, the second-generation system was much easier to use because the whole microlaparoscope could be sterilized and then quickly connected to the OSU in the operating room. In contrast, the first-generation system required careful placement of the sterilized polycarbonate housing over the nonsterile imaging catheter permanently connected to the OSU. The rigid stainless steel tubing solved the rigidity issues, enabling the surgeon to precisely position the device. A press of a button at the operator console enabled rapid delivery of a small droplet of contrast agent, as shown in Fig. 10. Focus was extremely reliable and never drifted. In fact, during typical use, the surgeon would set the focus at the epithelial surface and image multiple sites without needing to refocus.

Although the second-generation device addressed the primary issues encountered with the first-generation instrument, there were additional improvements that were important to make a successful clinical tool. Even though the manual focus system was reliable, a computerized system was desired to enable depth scans. Second, to allow the device to be controlled more efficiently by the surgeon, the microlaparoscope needed to integrate basic controls for focus, dye delivery, and data recording into the handle. The dye delivery system also needed some refinement. In the second-generation device, to ensure repeatable delivery of small contrast agent droplets, the pressure in the syringe had to be well regulated at a relatively high $1.76 \text{ kg}/\text{cm}^2$. This pressure would sometimes cause contrast agent to squirt out of the distal tip rather than pool up in a localized droplet.

2.2.3 Third-generation design

To implement these improvements, a third-generation device was developed. The new microlaparoscope, shown in Fig. 11, has an ergonomic handle, control buttons, a computerized focus system, and a refined contrast agent delivery system. Control of focus and dye delivery are consistent and reliable since

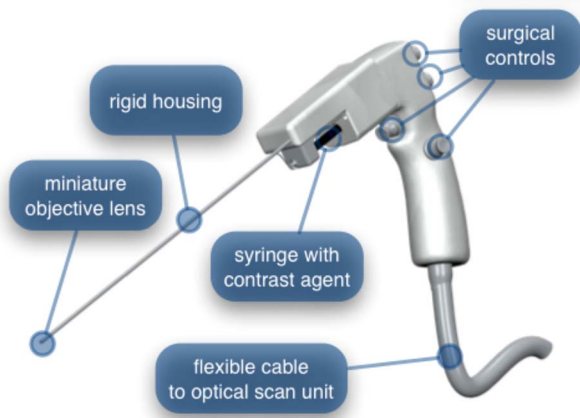


Fig. 11 The third-generation microlaparoscope. In this view, the rigid steel fiber bundle housing is visible entering into the main handle. A spring-loaded receptacle receives a 1-cm³ syringe loaded with contrast agents, which couples into the fluid line running to the distal tip. Four buttons allow the surgeon to control focus, contrast agent delivery, and data acquisition. A 6-m-long flexible line connects the microlaparoscope back to the OSU.

the control systems were miniaturized and located in the handle only 35 cm from the distal end of the device. A non-pressurized dye delivery system removed the problem encountered with dye ejection.

Mechanically, the third-generation microlaparoscope followed the same design principles as the second-generation device. Figure 12 illustrates the mechanical aspects of the device. The fiber bundle couples to the focus motor inside the handle. A 1-cm³ syringe with contrast agent is placed into a spring-loaded receiver at the front end of the handle. A second miniature motor in the handle acts as a plunger for the syringe. A spring forces the syringe to mate with a Luer Lock connection that guides the fluid down a 21-gauge hypodermic tube.

A customized tip helps to channel the dye and minimize tissue abrasion. The new tip is a 20-mm PEEK housing mated to the FEP outer tubing. A tiny 150- μ m lumen inside the PEEK couples the hypodermic fluid line routing the dye to an exit port at the edge of the system's field of view. In the second-generation design, the hypodermic tubing was bent around the tip of the miniature objective and had the potential to abrade the tissue surface. The new smooth tip helps to protect the tissue surface and allows the fluid exit port to be placed closer to the edge of the imaging field of view.

The handle contains four ergonomically positioned controls. Two upper thumb controls on the back allow the surgeon to adjust focus and acquire a depth scan. The trigger button saves still frames with a short press and acquires video with a long press. The side button delivers a predefined amount of contrast agent to the field of view.

The electrical wires and the fiber bundle are routed through the handle into a flexible 6-m protective cable. The rear end of the cable breaks out into an electrical connector and an SMA connector. Both connections couple to receptacles on the OSU. The electrical connection routes through the electronics of the OSU and exits as a single USB cable connecting to the computer which link the buttons and motors to the

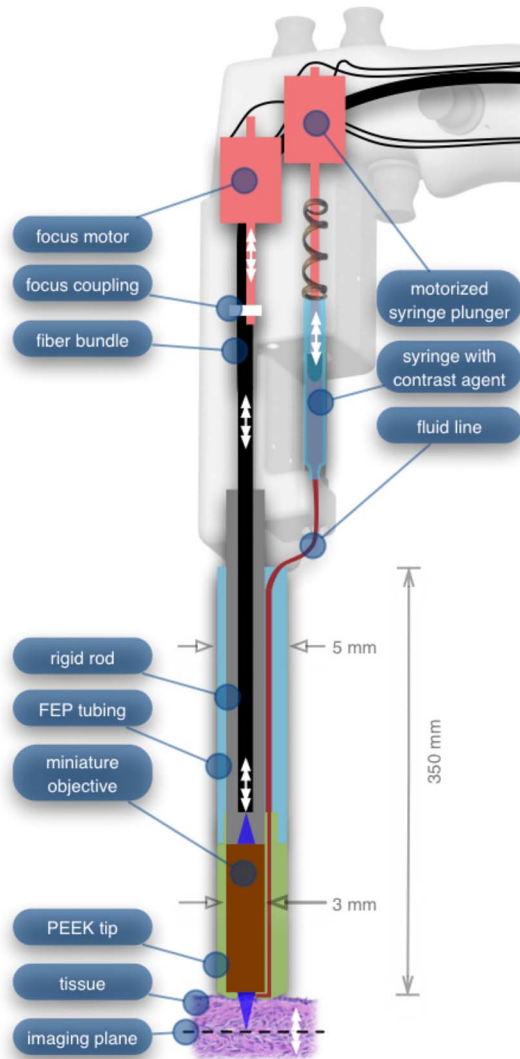


Fig. 12 Detailed cross-sectional view illustrating the focus mechanism and contrast agent delivery system in the third-generation microlaparoscope. The focus motor couples to the fiber bundle, causing axial movement of the distal end of the fiber relative to the lens. The motorized syringe plunger forces fluid in the syringe to pass through the fluid line, into the tip, and out the tiny orifice at the edge of the system's field of view. (Diagram not to scale.)

control software. The SMA connector couples the fiber bundle to the OSU.

The third-generation microlaparoscope represents a viable surgical tool. Its rigid probe enables precise positioning control. The in-handle computerized focus system enables axial focus and depth scans with accurate 1- μ m positioning. The contrast agent system delivers volumes with precision down to 50 nL. Last, the whole device has an ergonomic design that is comfortable for the surgeon to use and provides controls for all the tasks that the surgeon needs to perform.

3 Results

As previously mentioned, laparoscopic techniques can be used to access most organs in the body. To demonstrate the

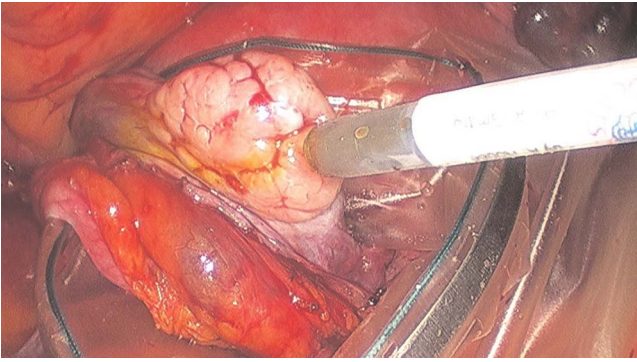


Fig. 13 Wide-field laparoscope view showing the second-generation microlaparoscope contacting the surface of the ovary. The organ, still attached to the blood supply, is laid inside an endobag to protect the patient from inadvertent exposure to contrast agents.

clinical viability of the confocal microlaparoscope system, we present results from two organs imaged using the device. The first set of results are *in vivo* and *ex vivo* images of the epithelial surface of ovarian tissue. Since there is no reliable way to detect ovarian cancer in its early stages,³⁷ the microlaparoscope could be used to detect ovarian cancer in high-risk women. The second set of results are *ex vivo* images of human esophagus. Although laparoscopic esophageal surgery is a recent innovation, it is now second only to biliary tract surgery in the frequency of minimally invasive procedures performed in everyday surgical practice.³⁸ The microlaparoscope's ability to visualize the cellular boundaries of tumors could improve the success rates in laparoscopic staging of carcinoma of the esophagus and laparoscopic esophagectomy.

3.1 Ovarian Images

Currently, the microlaparoscope is being evaluated in a clinical trial to image the epithelial surface of the ovary at the University of Arizona's Medical Center in Tucson. The device was granted "nonsignificant risk" status by the University of Arizona's Institutional Review Board and has been approved for use in humans using a protocol that includes topical application of contrast agents.³³ To date, 21 patients have been imaged *in vivo*.

The current protocol entails imaging human ovaries *in vivo* before oophorectomy or hysterectomy. The imaging protocol begins with the surgeon locating the ovary and isolating it in an endobag with the ovary still connected to the blood supply (see Fig. 13). Once the ovary is isolated, the surgeon brings the tip of the microlaparoscope into contact with the epithelial surface. Then the surgeon delivers the contrast agent, and live imaging begins. The endobag protects the patient from inadvertent exposure to contrast agent. After the microscopic imaging is done, the surgical procedure is completed as normal, and the ovaries are removed. The removed ovary is typically imaged again *ex vivo* using the microlaparoscope with additional contrast agents. Biopsies are also taken for correlated pathology.

For the initial *in vivo* clinical studies, fluorescein sodium was selected because of its existing track record of safe use in humans.^{39,40} (All patients participating in the clinical trials were consented and imaged in accordance with human sub-

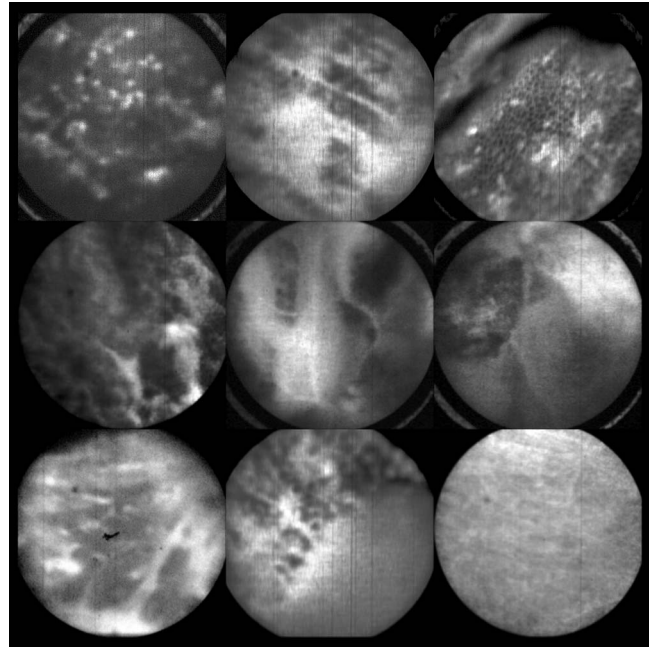


Fig. 14 Images of ovary epithelium obtained *in vivo* during clinical trials using fluorescein sodium. The low contrast is a result of the minimal preferential binding exhibited by fluorescein. (Circular field of view is 450 μm .)

jects protocols approved by the Institutional Review Board of the University of Arizona.) Although fluorescein provides limited diagnostic contrast when applied to the surface of the ovary, it is a safe contrast agent and allowed us to test the safety and basic functionality of the microlaparoscope system *in vivo*.

Figure 14 shows nine examples of *in vivo* images obtained with the microlaparoscope system. The images demonstrate that the device functions as designed. The microlaparoscope can deliver controlled volumes of dye to the image site and then display real-time cellular-level images to the surgeon. The focus mechanism works well. After an initial adjustment of the focus, the instrument can be moved to various sites on the ovary while still maintaining good focus on the epithelial surface.

After *in vivo* imaging with fluorescein, the surgeon removes the ovaries. The ovaries are reimaged *ex vivo* using acridine orange (AO). Compared to fluorescein, AO provides superior diagnostic contrast. Example images with AO, shown in Fig. 15, demonstrate the excellent cellular-level contrast achievable with the instrument. The epithelial surface of a healthy ovary is characterized by a homogeneous distribution of bright nuclei, as seen in Fig. 15(a). The epithelial surface cells of the ovary are delicate, and partial denuding can occur, exposing the underlying stroma [Fig. 15(b)]. Below the epithelial surface, healthy stroma also exhibits a characteristically homogenous structure albeit with a different nuclear size distribution and shape [Fig. 15(c)]. In the case of ovarian cancer, the tissue structure is visibly different [Fig. 15(d)]. The epithelial surface is irregular, and the high degree of heterogeneity in the size and spatial distribution of nuclei is indicative of ovarian cancer.

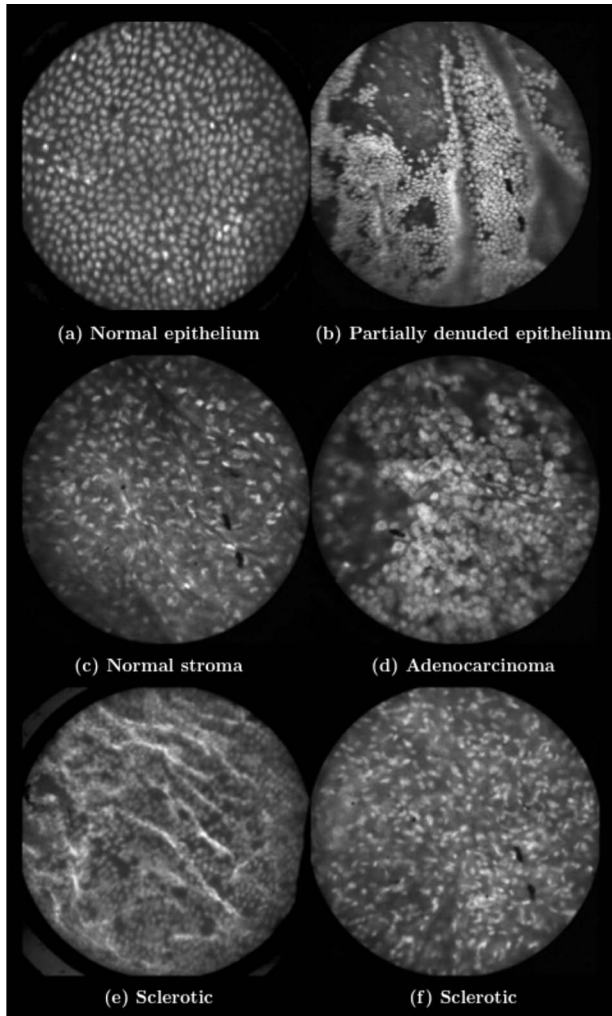


Fig. 15 Images of human ovary epithelium obtained *ex vivo* using AO. Subcaptions contain pathology diagnosis. (Circular field of view is $450\ \mu\text{m}$.)

We have previously shown⁴¹ that the microlaparoscope system can easily differentiate between normal epithelium and ovarian cancer using automated algorithms. It also appears that the microlaparoscope system may be able to visualize cellular changes that happen prior to the onset of cancer. Less distinct tissue changes such as tissue sclerosis may also be detectable [Figs. 15(e) and 15(f)].

With the success of our initial testing with fluorescein, we have now begun imaging *in vivo* with AO. (Approval from the FDA to use AO in this context has been granted under IND 102603.) Figure 16 shows our preliminary results. These images depict the same homogeneous structure of nuclei as seen in Figs. 15(a) and 15(b). Denuding of the delicate epithelium is also visible in some of the images. By optimizing the concentration of AO and giving surgeons more time to practice using the device, we believe we will achieve results comparable to the images obtained *ex vivo*.

3.2 Esophagus Images

We have conducted *ex vivo* imaging of esophagus tissue biopsies from more than 30 patients. Figure 17(a) shows an

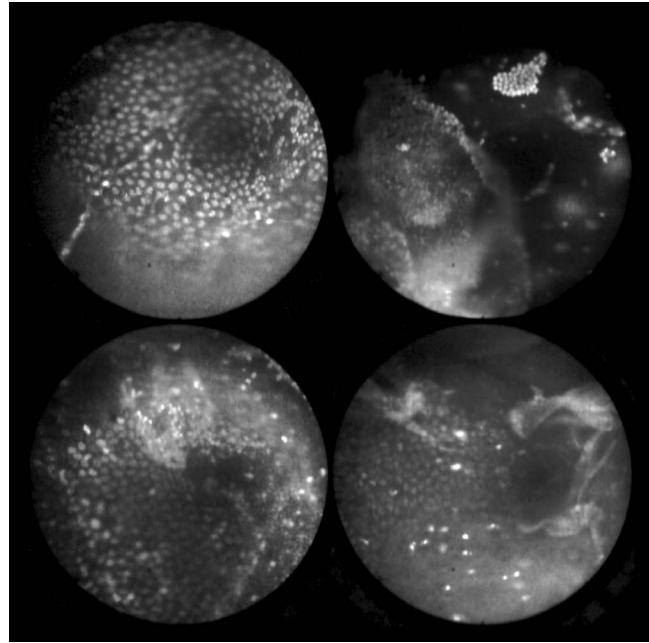


Fig. 16 Images of ovary epithelium obtained *in vivo* during clinical trials using AO at $330\ \mu\text{mol/L}$. (Circular field of view is $450\ \mu\text{m}$.)

example of normal squamous epithelium. Figure 17(b) shows epithelial tissue that closely resembles the intestine, with columnar-appearing mucosa and intestinal metaplasia, a condition known as Barrett's esophagus. Finally, Fig. 17(c) illustrates a tumor in the esophagus.

These images illustrate the device's ability to resolve the cellular details of tissue in the esophagus. Nuclear distributions are easily characterized, and morphological tissue changes can be readily discerned. In the case of laparoscopic esophagectomy, the microlaparoscope would allow the surgeon to optically biopsy suspect tissues to potentially find locations containing cancer.

4 Conclusions and Future Work

A mobile confocal microlaparoscope system capable of performing live optical biopsies *in vivo* has been developed. The system is currently being evaluated in clinical trials to assess its safety and efficacy for detecting ovarian cancer. Results show that the instrument is safe and can successfully image ovaries *in vivo*.

The *in vivo* and *ex vivo* results indicate that the microlaparoscope can resolve sufficient cellular detail to detect the transformation of normal epithelium and visualize cellular changes that happen with the onset of cancer. As we continue testing, we hope to show that the device can obtain the same high-quality images *in vivo* as have been obtained *ex vivo*.

Because the microlaparoscope can nondestructively provide real-time cellular images *in vivo*, it has the potential to significantly improve the rate of early cancer detection in laparoscopically accessible organs. Today, early detection of cancer is highly dependent on the selection of biopsy sites. Since biopsies are destructive, only a few are typically taken. If cancer is in its early stages, it will often be small, reducing the probability that it will be biopsied. Moreover, it takes time to

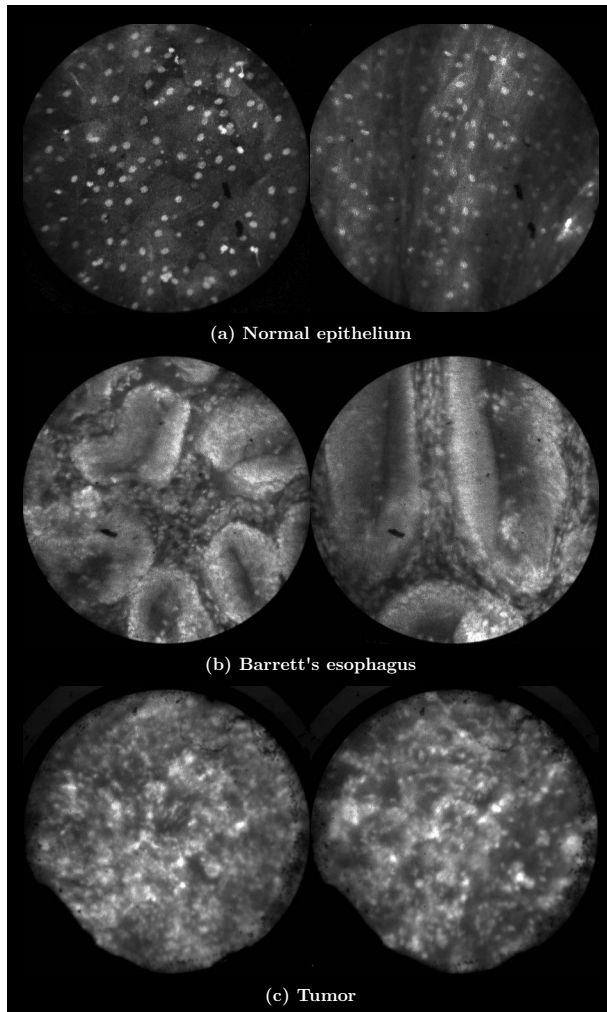


Fig. 17 Images of human esophagus epithelium obtained *ex vivo* using AO. Subcaptions contain pathology diagnosis. (Circular field of view is 450 μm .)

get the biopsies processed and evaluated. However, because the microlaparoscope nondestructively acquires optical biopsies instantly, a much larger region of tissue can be interrogated at the cellular level. Additionally, if the surgeon finds a small cancer, the microlaparoscope could be used to locate the cancer boundaries allowing for immediate resection. Thus, the device might improve the probability of early cancer detection and help the surgeon fully resect the tumor during the same procedure.

In the future, we will continue to investigate the wide range of potential applications for the confocal microlaparoscope system. Since the microlaparoscope is based on an inherently flexible fiber bundle, we plan on making a device with a flexible probe. We have previously shown a flexible imaging catheter and plan to apply the technology developed for the microlaparoscope to a new confocal microgastroscope for interrogating the gastrointestinal tract.

Acknowledgments

The authors wish to acknowledge the contribution of Dr. Molly Brewer, Dr. Richard Sampliner, Kathy Schmidt, and

the surgical staff at UMC. Dr. Brewer helped motivate the development of the instrument and gave guidance on how such an instrument would be used in a clinical setting. Dr. Sampliner provided human esophagus biopsies for the *ex vivo* imaging studies. Kathy Schmidt and the surgical staff provided valuable assistance in the clinical trials. Last, we recognize the National Institutes of Health and the Arizona Disease Control Research Commission for their funding support provided through the following grants: NIH CA 73095, NIH CA 115780, and ADCRC 9711.

References

1. L. J. Kleinsmith, *Principles of Cancer Biology*, Pearson Benjamin Cummings, San Francisco (2006), <http://www.loc.gov/catdir/toc/ecip0511/2005010378.html>.
2. T. Wang, M. Mandella, C. Contag, and G. Kino, "Dual-axis confocal microscope for high-resolution *in vivo* imaging," *Opt. Lett.* **28**, 414–416 (2003).
3. R. Kiesslich, L. Gossner, M. Goetz, A. Dahlmann, M. Vieth, M. Stolte, A. Hoffman, M. Jung, B. Nafe, P. Galle, and M. F. Neurath, "In vivo histology of Barrett's esophagus and associated neoplasia by confocal laser endomicroscopy," *Nat. Clin. Pract. Gastroenterol. Hepatol.* **4**, 979–987 (2006).
4. A. Polglase, W. McLaren, S. Skinner, R. Kiesslich, M. Neurath, and P. Delaney, "A fluorescence confocal endomicroscope for *in vivo* microscopy of the upper- and the lower-GI tract," *Gastrointest. Endosc.* **62**, 686–695 (2005).
5. C. Boudoux, S. Yun, W. Oh, W. White, N. Iftimia, M. Shishkov, B. Bouma, and G. Tearney, "Rapid wavelength-swept spectrally encoded confocal microscopy," *Opt. Express* **13**, 8214–8221 (2005).
6. A. Gerger, S. Koller, T. Kern, C. Massone, K. Steiger, E. Richtig, H. Kerl, and J. Smolle, "Diagnostic applicability of *in vivo* confocal laser scanning microscopy in melanocytic skin tumors," *J. Invest. Dermatol.* **124**, 493–498 (2005).
7. Y. Kakeji, S. Yamaguchi, D. Yoshida, K. Tanoue, M. Ueda, A. Masunari, T. Utsunomiya, M. Imamura, H. Honda, Y. Maehara, and M. Hashizume, "Development and assessment of morphologic criteria for diagnosing gastric cancer using confocal endomicroscopy: an *ex vivo* and *in vivo* study," *Endoscopy* **38**, 886–890 (2006).
8. N. Nguyen and R. Leong, "Current application of confocal endomicroscopy in gastrointestinal disorders," *J. Gastroenterol. Hepatol* **23**, 1483–1491 (2008).
9. Y.-T. Guo, Y.-Q. Li, T. Yu, T.-G. Zhang, J.-N. Zhang, H. Liu, F.-G. Liu, X.-J. Xie, Q. Zhu, and Y.-A. Zhao, "Diagnosis of gastric intestinal metaplasia with confocal laser endomicroscopy *in vivo*: a prospective study," *Endoscopy* **40**, 547–553 (2008).
10. M. Nakao, S. Yoshida, S. Tanaka, Y. Takemura, S. Oka, M. Yoshihara, and K. Chayama, "Optical biopsy of early gastroesophageal cancer by catheter-based reflectance-type laser-scanning confocal microscopy," *J. Biomed. Opt.* **13**, 054043 (2008).
11. K. Konig, A. Ehlers, I. Riemann, S. Schenkl, R. Buckle, and M. Kaatz, "Clinical two-photon microendoscopy," *Microsc. Res. Tech.* **70**, 398–402 (2007).
12. S. Zhuo, J. Chen, T. Luo, X. Jiang, S. Xie, and R. Chen, "Two-layered multiphoton microscopic imaging of cervical tissue," *Lasers Med. Sci.* **24**, 359–363 (2008).
13. R. Richards-Kortum, N. Ramanujam, A. Mahadevan-Jansen, M. Follen, and U. Utzinger, "Method for probabilistically classifying tissue *in vitro* and *in vivo* using fluorescence spectroscopy," U.S. Patent No. 7,236,815 (2007).
14. U. Utzinger and R. Richards-Kortum, "Fiber optic probes for biomedical optical spectroscopy," *J. Biomed. Opt.* **8**(1), 121–147 (2003).
15. A. S. Haka, K. E. Shafer-Peltier, M. Fitzmaurice, J. Crowe, R. R. Dasari, and M. S. Feld, "Diagnosing breast cancer by using Raman spectroscopy," *Proc. Natl. Acad. Sci. U.S.A.* **102**, 12371–12376 (2005).
16. J. T. Motz, S. J. Gandhi, O. R. Scepanovic, A. S. Haka, J. R. Kramer, R. R. Dasari, and M. S. Feld, "Real-time Roman system for *in vivo* disease diagnosis," *J. Biomed. Opt.* **10**, 031113 (2005).
17. J. A. Freeberg, J. L. Benedet, C. MacAulay, L. A. West, and M. Follen, "The performance of fluorescence and reflectance spectroscopy for the *in vivo* diagnosis of cervical neoplasia; point probe ver-

- sus multispectral approaches," *Gynecol. Oncol.* **107**, S248–S255 (2007).
18. P. Mayes, D. Dicker, Y. Liu, and W. El-Deiry, "Noninvasive vascular imaging in fluorescent tumors using multispectral unmixing," *Bio-Techniques* **45**, 459–464 (2008).
 19. A. Tumlinson, J. Barton, B. Považay, H. Sattman, A. Unterhuber, R. Leitgeb, and W. Drexler, "Endoscope-tip interferometer for ultrahigh resolution frequency domain optical coherence tomography in mouse colon," *Opt. Express* **14**, 1878–1887 (2006).
 20. G. Tearney, S. Boppart, B. Bouma, M. Brezinski, N. Weissman, J. Southern, and J. Fujimoto, "Scanning single-mode fiber optic catheter-endoscope for optical coherence tomography," *Opt. Lett.* **21**, 543–545 (1996).
 21. P. Wilder-Smith, W.-G. Jung, M. Brenner, K. Osann, H. Beydoun, D. Messadi, and Z. Chen, "In vivo optical coherence tomography for the diagnosis of oral malignancy," *Lasers Surg. Med.* **35**, 269–275 (2004).
 22. Z. Wang, C. Lee, W. Waltzer, Z. Yuan, Z. Wu, H. Xie, and Y. Pan, "Optical coherence tomography for noninvasive diagnosis of epithelial cancers," in *Conf. Proc. IEEE Eng. Med. Biol. Soc.*, Vol. **1**, pp. 129132 (2006).
 23. Y. Chen et al., "Ultrahigh resolution optical coherence tomography of Barrett's esophagus: preliminary descriptive clinical study correlating images with histology," *Endoscopy* **39**, 599–605 (2007).
 24. S. Lam, B. Standish, C. Baldwin, A. McWilliams, J. leRiche, A. Gazdar, A. I. Vitkin, V. Yang, N. Ikeda, and C. MacAulay, "In vivo optical coherence tomography imaging of preinvasive bronchial lesions," *Clin. Cancer Res.* **14**, 2006–2011 (2008).
 25. P.-A. Testoni and B. Mangiavillano, "Optical coherence tomography in detection of dysplasia and cancer of the gastrointestinal tract and bilio-pancreatic ductal system," *World J. Gastroenterol.* **14**, 6444–6452 (2008).
 26. A. F. Gmitro and D. Aziz, "Confocal microscopy through a fiber-optic imaging bundle," *Opt. Lett.* **18**, 565–567 (1993).
 27. H. Makhlof, A. F. Gmitro, A. A. Tanbakuchi, J. A. Udovich, and A. R. Rouse, "Multispectral confocal microendoscope for *in vivo* and *in situ* imaging," *J. Biomed. Opt.* **13**, 044016 (2008).
 28. Y. S. Sabharwal, A. R. Rouse, L. Donaldson, M. F. Hopkins, and A. F. Gmitro, "Slit-scanning confocal microendoscope for high-resolution *in vivo* imaging," *Appl. Opt.* **38**, 7133–7144 (1999).
 29. A. R. Rouse and A. F. Gmitro, "Multispectral imaging with a confocal microendoscope," *Opt. Lett.* **25**, 1708–1710 (2000).
 30. A. R. Rouse, A. Kano, J. A. Udovich, S. M. Kroto, and A. F. Gmitro, "Design and demonstration of a miniature catheter for a confocal microendoscope," *Appl. Opt.* **43**, 5763–5771 (2004).
 31. K. A. Zucker, Ed., *Surgical Laparoscopy*, Lippincott Williams & Wilkins, Hagerstown, MD (1991).
 32. A. Tanbakuchi, A. Rouse, K. Hatch, R. Sampliner, J. Udovich, and A. Gmitro, "Clinical evaluation of a confocal microendoscope system for imaging the ovary," *Endoscopic Microscopy III, Proc. SPIE* **6851**, 685103 (2008).
 33. J. A. Udovich, A. R. Rouse, A. Tanbakuchi, M. A. Brewer, R. Sampliner, and A. F. Gmitro, "Confocal micro-endoscope for use in a clinical setting," *Proc. SPIE* **6432**, 64320H (2007).
 34. A. A. Tanbakuchi, A. R. Rouse, J. A. Udovich, and A. F. Gmitro, "Surgical imaging catheter for confocal microendoscopy with advanced contrast delivery and focus systems," *Proc. SPIE* **6082**, 608202 (2006).
 35. A. R. Rouse, A. A. Tanbakuchi, J. A. Udovich, and A. F. Gmitro, "Design of an *in vivo* multi-spectral confocal microendoscope for clinical trials," *Proc. SPIE* **6082**, 608205, <http://link.aip.org/link/?PSI/6082/608205/1> (2006).
 36. H. Makhlof, A. A. Tanbakuchi, A. R. Rouse, and A. F. Gmitro, "Design of multi-spectral channel for *in vivo* confocal microscopy," *Proc. SPIE* **6432**, 643206, <http://link.aip.org/link/?PSI/6432/643206/1> (2007).
 37. B. S. Kramer, J. Gohagan, and P. C. Prorok, "NIH consensus 1994: screening," *Gynecol. Oncol.* **55**, S20–S21 (1994).
 38. D. Bowrey and J. Peters, "Laparoscopic esophageal surgery," *Surg. Clin. North Am.* **80**, 1213–1242 (2000).
 39. K. Lange and L. Boyd, "The use of fluorescein to determine the adequacy of the circulation," *Med. Clin. North Am.* **26**, 943–952 (1942).
 40. M. Morykwas, H. Hills, and L. Argenta, "The safety of intravenous fluorescein administration," *Ann. Plast. Surg.* **26**, 551–553 (1991).
 41. S. Srivastava, J. Rodríguez, A. Rouse, M. Brewer, and A. Gmitro, "Computer-aided identification of ovarian cancer in confocal microendoscope images," *J. Biomed. Opt.* **13**, 024021 (2008).